PHILIPPINE ENGINEERING JOURNAL
PEJ 2025; Vol. 46, No. 2: 44-58

Received: 16 July 2025
Received in Revised Form: 15 August 2025
Accepted: 05 November 2025

Cellulose Microfiber Membranes Loaded with Magnetite Nanoparticles from Sugarcane Bagasse for Efficient Rhodamine B Degradation via Peroxymonosulfate Activation

Joanne B. Rafael and Eden May B. Dela Peña*
Department of Mining, Metallurgy, and Materials Engineering, University of the Philippines Diliman
**Corresponding author: ebdelapena@up.edu.ph*

Abstract *– The growing demand for efficient and sustainable water treatment technologies has prompted the exploration of biomaterial-based catalysts. This study investigates the synthesis and performance of magnetic cellulose microfiber membranes (MGCMFs) derived from sugarcane bagasse, an abundant agricultural waste in the Philippines, for the degradation of Rhodamine B (RhB) through peroxymonosulfate (PMS) activation. Cellulose microfiber (CMF) were extracted via alkaline delignification and mechanical fibrillation. Magnetite nanoparticles (MNPs) were synthesized onto the CMF using a co-precipitation method at varying precursor concentrations. Characterizations using SEM, Raman, FTIR, and XRD confirmed successful incorporation of MNPs with nanoscale features and magnetic properties. The MGCMF with low MNP content (MGCMF1) exhibited 97.81% RhB degradation within 300 minutes, outperforming both the high MNP-loaded (MGCMF2) and non-magnetic CMF membranes. Kinetic analysis revealed that MGCMF1 followed pseudo-first-order and Langmuir-Hinshelwood models, indicating surface catalysis. These findings suggest that the sugarcane-derived MGCMFs offer a promising, eco-friendly solution for dye-polluted water remediation.*

Keywords*: magnetic cellulose, textile wastewater, sugarcane bagasse*

I. INTRODUCTION

Synthetic organic dyes are widely used in the manufacture of a wide range of colorful products, including textiles, paper, cosmetics, and pharmaceuticals. However, these chemicals often end up in industrial effluents, becoming major contributors to water pollution. Organic dyes are not only persistent in aquatic environments but also toxic, posing risks to aquatic organisms such as fish, algae, and invertebrates. They also threaten human health through exposure pathways such as contaminated drinking water and ingestion, potentially leading to endocrine disruption, as well as carcinogenic and mutagenic effects [1]. One notable example is Rhodamine B (RhB), which is carcinogenic and can damage human organs with prolonged exposure [1]. The threat posed by RhB and various other synthetic organic dyes necessitates the development of advanced water treatment methods.

Advanced oxidation processes (AOPs) have emerged as an effective strategy for degrading organic pollutants. AOPs are based on generating highly reactive radicals that non-selectively oxidise and break down most organic species in water into less harmful compounds [2, 3]. Among these, peroxymonosulfate (HSO_5^- or PMS)-based AOPs are of special interest due to

their ability to produce sulfate ($SO_4 \cdot^-$) and hydroxyl radicals (·OH) [4, 5]. Sulfate radicals are generated through the activation of PMS—via heat, transition metals, UV light, or alkaline conditions—according to reactions such as:

$$HSO_5^- + Fe^{2+} \rightarrow SO_4 \cdot^- + Fe^{3+} + OH^- \quad (1)$$

Hydroxyl radicals can be formed either directly from PMS activation or indirectly through the reaction of sulfate radicals with water or hydroxide ions:

$$SO_4 \cdot^- + H_2O \rightarrow \cdot OH + HSO_4^- \quad (2)$$
$$SO_4 \cdot^- + OH^- \rightarrow \cdot OH + SO_4^{2-} \quad (3)$$

In this system, PMS needs to be activated by some external agent or catalysts, including heat, ultraviolet (UV) radiation, transition metals and magnetic nanoparticles [4]. One popular magnetic catalyst is magnetite nanoparticles (nano-Fe_3O_4 or MNP) [4-7]. Magnetite nanoparticles are attractive in wastewater treatment due to their high adsorption surface, inexpensive production cost, and stable chemical structure [7, 8]. Additionally, these particles can be separated and recovered in the downstream using an external magnetic field. This magnetic recoverability also presents opportunities for the reusability and recyclability of MGCMF membranes, which are important considerations for sustainable and cost-effective applications [9, 10].

While magnetite nanoparticles were proven effective, the use of bare nanoparticles has some inherent limitations. At high concentrations, the dispersed nanoparticles tend to aggregate, creating large particles that settle and thereby reduce their catalytic efficiency [11]. To overcome this, attaching MNP on biocompatible templates or substrates such as cellulose, chitosan and gelatin has been proposed [10]. Cellulose, particularly the nanocellulose form, is attractive as it is cheap and abundant, renewable, and biodegradable [12]. Several studies have reported good results from the MNP-nanocellulose combination when used as a catalyst in AOPs. For example, Amiralian et al. [13] fabricated MNP-loaded nanocellulose and used this to activate peroxymonosulphate (PMS) to remove Rhodamine B (RhB). They reported a dye degradation efficiency of 94.9% after 300 min of oxidation at room temperature. Ariaeenejad et al. [14] fabricated magnetic Fe/nanocellulose hybrids and used them as a catalyst in a H_2O_2-based AOP. They measured removal efficiencies of 98%, 96% and 62% for methylene blue, crystal violet, and congo red dyes.

Although nanocellulose is generally considered effective, safe and biocompatible, concerns remain regarding some potential adverse effects, specifically after long-term exposures. From a wastewater treatment perspective, any unrecovered nanocellulose used in a treatment step can easily go undetected because of its size. This can then re-enter potable water streams and potentially be ingested by people. To address this issue, a proposed solution is to use a larger form of cellulose, called cellulose microfiber (CMF). Beyond being easier to detect and recover in the wastewater stream, CMF offer higher mechanical stability, lower separation challenges, and reduced health and environmental risks compared to nanocellulose. They can also be produced more cost-effectively from agricultural wastes such as rice husks, wheat

straw, and sugarcane bagasse [15]. From a processing perspective, producing CMF is less intensive compared to producing nanocellulose, which can lead to reduced production costs.

Currently, there are very few reports on using magnetic particle-loaded CMF in a PMS system to treat synthetic dyes. Basic questions on the material's feasibility, suitability in PMS activation, and dye degradation efficiency need to be answered. This study aims to address this research gap. A magnetite nanoparticle-cellulose microfiber membranes (MGCMFs) was fabricated using Philippine sugarcane bagasse as cellulose source. The membrane will be characterized and assessed for its effectiveness in degrading the representative pollutant dye, Rhodamine B, within a PMS-based AOP system. Additionally, the valorization of agricultural waste, such as sugarcane bagasse, contributes to circular economy practices by converting low-value residues into high-value products, thereby reducing waste, conserving resources, and supporting sustainable development goals [16]. The Philippines generates substantial amounts of sugarcane waste annually, making it a suitable candidate for conversion into high-value materials. The integration of cellulose with magnetic nanoparticles creates a hybrid system capable of acting as both a sorbent and a catalyst for dye degradation. Such multifunctional materials are key in addressing water pollution in a cost-effective and environmentally conscious manner.

II. METHODOLOGY

2.1. Materials

Sugarcane bagasse was collected from a local source. Reagents used include sodium hydroxide (NaOH), glacial acetic acid (CH_3COOH, $NaClO_2$), sodium chlorite- Technical Grade 80% (NaClO2), ammonium hydroxide 25wt% (NH_4OH), ferric (III) chloride hexahydrate 96% ($FeCl_3 \cdot 6H_2O$), ferrous (II) chloride 98% ($FeCl_2$), peroxymonosulphate (PMS), and Rhodamine (RhB). All solutions were prepared using deionised water.

2.2. Extraction of Cellulose Microfiber

The sugarcane bagasse was washed, air-dried, ground, and sieved. The sieved fibers were delignified in 2% NaOH at 80°C, bleached with 1% $NaClO_2$ at 70 °C (pH adjusted to 4), and then oven-dried. The pulp was then mechanically fibrillated via sonication and homogenization to yield the microcellulose fibers. This process removed lignin and hemicellulose, exposing hydroxyl groups essential for nanoparticle anchoring.

2.3. Synthesis of Magnetic Cellulose Microfiber

Magnetite nanoparticles (MNP) were synthesized onto the CMF using a co-precipitation process under a nitrogen atmosphere. The co-precipitation method offers the advantage of uniform distribution of nanoparticles while minimizing oxidation [17]. Two types of specimens were prepared by changing the amount of Fe^{3+} (from $FeCl_3 \cdot 6H_2O$) and Fe^{2+} (from $FeCl_2$) precursors. For the first specimen, referred to as MGCMF1, 2.2g and 0.45g of Fe^{3+} and Fe^{2+} precursors were added, respectively. For the second specimen, MGCMF2, the concentrations of precursors were double those of MGCMF1. 25% NH_4OH solution was added dropwise to precipitate Fe_3O_4 in situ. After precipitation, a black product was obtained. The

precipitate was collected via normal gravity filtration using filter paper, washed with distilled water, and air dried.

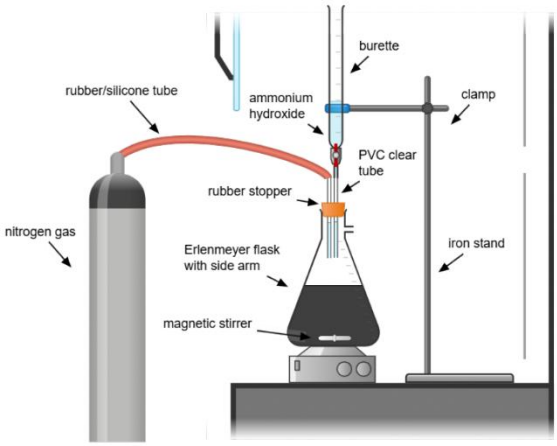

Figure 1. Experimental setup for the synthesis of magnetite nanoparticles.

2.4. Dye Degradation Tests

For the dye degradation test, flat membranes were used. These membranes were formed from the dried MGCMF using a hydraulic hot press (110 °C, 10 MPa, 1.5 h). RhB degradation tests were conducted using 20 mg of the pressed membrane in 100 mL of 20 mg/L RhB solution with 100 mg PMS. Each experiment was performed in triplicate to ensure repeatability, and the results were statistically reproducible within the reported error ranges. Samples were taken every 30 minutes and analyzed at 554 nm using a UV–Vis spectrophotometer. Control experiments were conducted using only CMF to isolate the catalytic effect of the MNP.

2.5. Characterization of MGCMF

Scanning electron microscope (SEM, Hitachi SU3500) was used to image the surface morphology of the specimen. Raman spectroscopy (Horiba LabRAM HR) and Fourier Transform Infrared (FTIR, Nicolet iS50) spectroscopy were used to confirm the presence of functional groups in the cellulose.

X-ray diffraction analysis (Shimadzu XRD 7000) was conducted to detect the presence of Fe_3O_4 and cellulose. The MNP particle size was calculated from the XRD spectrum using Scherrer's equation [18]. The crystallinity index, I_{cr} of cellulose was calculated from the XRD spectrum using Segal's equation [19]:

$$I_{cr} = \frac{I_c - I_{am}}{I_c} \text{x} 100\% \quad (4)$$

where I_c is the intensity at the peak $2\theta \sim= 22°$ corresponding to the crystalline region of cellulose, and I_{am} is the intensity at the peak $2\theta \sim=15°$ corresponding to the amorphous region of cellulose.

III. RESULTS AND DISCUSSION

3.1. Magnetic Cellulose Microfiber Characterization

Figure 2 shows the SEM micrographs of the pure cellulose microfiber (CMF), pure magnetite nanoparticles (MNP), and the two magnetic cellulose microfiber specimens, MGCMF1 and MGCMF2. The extracted CMF exhibited a smooth surface, indicative of delignification that occurred after the applied chemical treatments [20]. The size of the cellulose fibers is in the micrometer scale. Measurements using ImageJ, obtained by analyzing SEM micrographs with the software's line tool calibrated to the image scale bar, show that the CMF diameters range from 4.9 to 18.8μm. The presence of smaller fibrils was also detected with diameters ranging from 0.34 to 0.4μm. This indicates that the ultrasonication step was successful in disintegrating the fibers to the desired degree, and such would also increase their surface area [21].

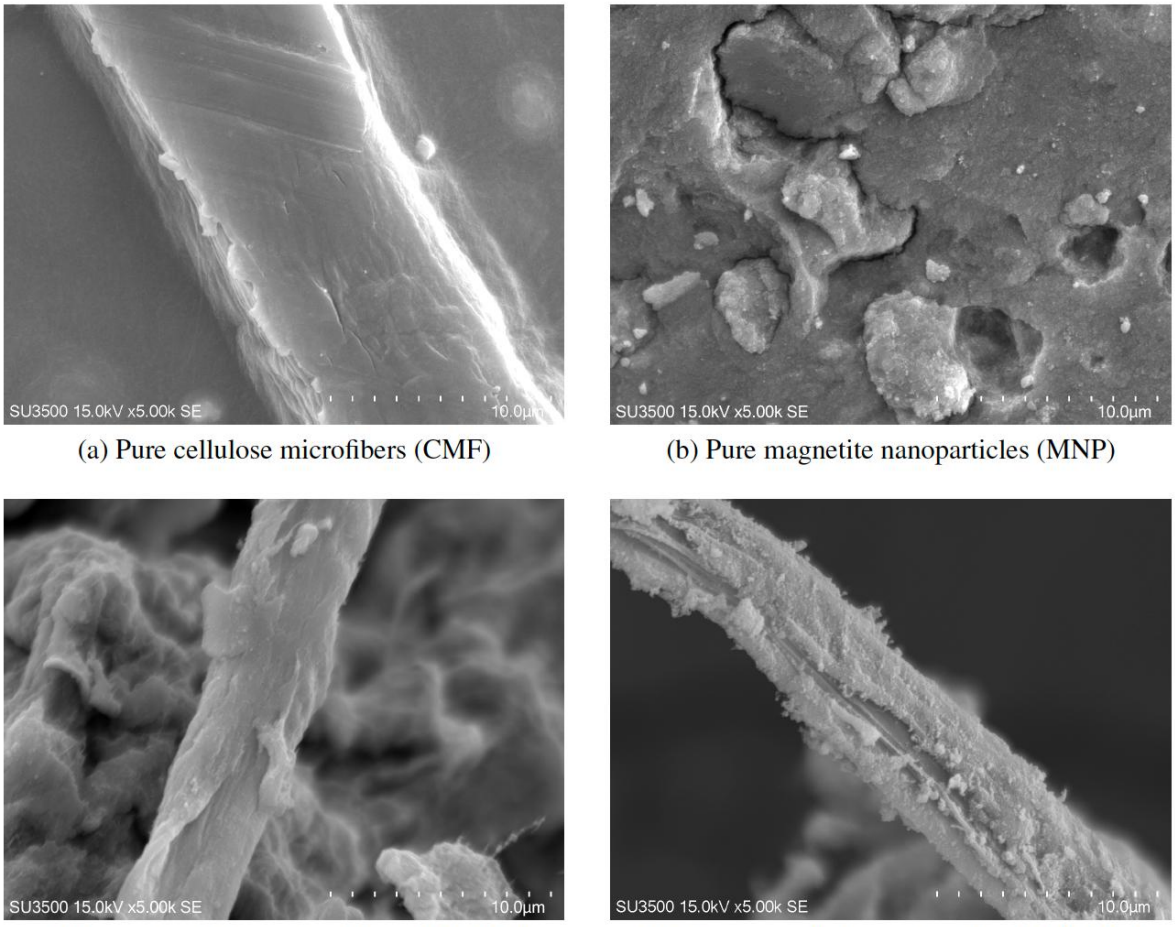

(a) Pure cellulose microfibers (CMF)

(b) Pure magnetite nanoparticles (MNP)

(c) Magnetic cellulose microfiber (MGCMF1)

(d) Magnetic cellulose microfiber (MGCMF2)

Figure 2. SEM micrographs (15.0kV, 5.00k magnification) for (a) pure cellulose microfiber (CMF), (b) pure magnetite nanoparticles (MNP), (c) magnetic cellulose microfiber (MGCMF1), and magnetic cellulose microfiber (MGCMF2).

The fabricated MNP appear agglomerated, as seen in Figure 2b. Although the size of individual nanoparticles is not apparent in this image, estimates of their sizes were obtained using XRD (this will be discussed in a subsequent section). Figure 2c shows that the magnetite nanoparticles were successfully grafted onto the surface of the microfiber. While the MGCMF1 sample appears smooth, the MGCMF2 sample exhibits a flakey appearance. Given that MGCMF2 contains twice the amount of added precursors, this morphology suggests that the MNPs likely aggregated and formed a continuous coating over the microfiber surfaces. This coating could account for the more pronounced brittleness observed in the MGCMF2 membranes compared to MGCMF1. MGCMF2 was noticeably fragile and prone to breaking easily during handling and experimental procedures, likely reflecting the inherent rigidity and poor ductility of the MNPs.

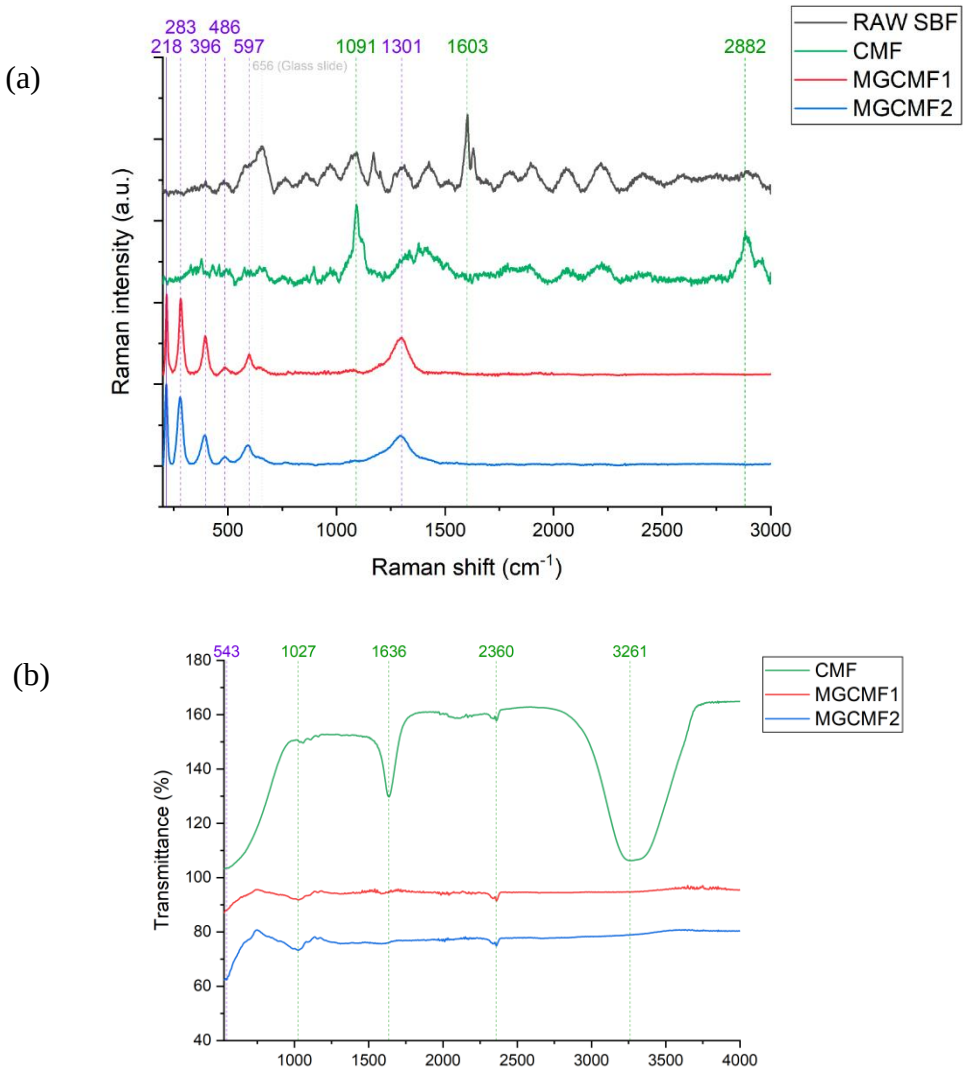

Figure 3. (a) Raman spectrum of raw sugarcane bagasse fiber (SBF), CMF, MGCMF1, and MGCMF2. (b) FTIR spectrum of CMF, MGCMF1, and MGCMF2.

Raman spectroscopy was used to detect the molecular compounds present across the different stages of MGCMF fabrication. The obtained Raman spectra of the specimens are shown in Figure 3(a). For the raw sugarcane bagasse fiber (RAWSBF) spectra, a strong peak at 1603 cm^{-1} is observed, attributed to phenyl groups present in lignin [22]. This peak subsequently disappeared in the CMF sample, confirming that lignin was successfully removed after the chemical treatments and cellulose extraction [23]. The peaks at 1091 and 2882 cm^{-1} were also more prominent in the CMF spectrum compared to those in the raw bagasse fiber spectrum. These two peaks coincide with the peaks for cellulose and hemicellulose, respectively [24]. This means that the delignification process was successful in extracting cellulose and hemicellulose. However, this also meant that remnants of hemicellulose were not fully removed, which is undesirable in cellulose extraction. Thus, additional treatments or longer processing times may be applied to the raw sugarcane bagasse fibers to fully isolate the cellulose in future extractions. In the MGCMF1 and MGCMF2 the peaks seen at 396, 486, and 597 cm^{-1} were prominent. These peaks correspond to the vibration modes of the Fe-O bonds, confirming the successful synthesis of the Fe_3O_4 NPs [25]. Meanwhile, the bands at 218, 283, and 1301 cm^{-1} correspond to hematite (α-Fe_2O_3), whose characteristic Raman peaks typically appear at ~225, 245, 293, 299, 412, 499, 613, and 1315 cm^{-1}. In contrast, magnetite (Fe_3O_4) exhibits prominent peaks around ~670 cm^{-1} and ~540 cm^{-1}, which are absent or significantly reduced in the present spectra. This clear shift in peak positions and intensities suggests a partial phase transformation from magnetite to hematite, likely due to oxidation of the particles during Raman testing, induced by the laser-related temperature rise of the samples [25-26]. A study by Shebanova & Lazor [26] reported that the intensity of these peaks increased with laser power, with rapid oxidation occurring even below 25mW, making it challenging to prevent [26].

The FTIR spectra of CMF, MGCMF1, and MGCMF2 is shown in Figure 4(b). The FTIR analysis reveal distinct transmittance bands at 3261, 2360, 1636, and 1027 cm^{-1} across all samples. These bands correspond to (i) the stretching vibrations of hydroxyl groups (-OH), which is indicative of the primary functional groups in lignocellulosic materials; (ii) the -CH stretching vibrations in methylene groups; (iii) the bending vibrations of hydroxyl groups (-OH) from absorbed water; (iv) and the stretching vibrations of C-O-C in the pyranose rings found in lignin, respectively.

A slightly prominent peak at 543 cm^{-1}, which likely corresponds to the Fe-O stretching vibrations in the tetrahedral site, was detected in the two MGCMF specimens and confirms the presence of magnetite [27]. While additional peaks related to the MNP was anticipated, however, the small amount of MNP and the inherent limitations of the FTIR equipment likely contributed to the absence of other peaks corresponding to the iron oxide. The transmittance band at 3261 cm^{-1} attributed to the cellulose microfiber is also not clearly visible in the MGCMF samples. This may be due to interactions and bond formation between the hydroxyl groups of cellulose microfiber and the magnetic nanoparticles, which could have weakened the O-H stretching vibrations in the spectra [28]. Furthermore, the low initial concentration of cellulose microfiber (0.3% w/v) in the dispersion during synthesis likely contributed to the poor resolution of their characteristic spectral features.

The XRD patterns of CMF, MGCMF1, and MGCMF2 are displayed in Figure 4, and the corresponding spectra exhibit peaks characteristic of both the cellulose microfiber and the magnetite nanoparticles. Cellulose is a polymeric material exhibiting a semi-crystalline structure.

For the CMF sample, two prominent peaks at 22.12° and 15.83°, corresponding to the (002) and (110) lattice planes, respectively, are characteristic of cellulose [13, 29]. These specific peaks were selected because they are commonly reported as the primary reflections for cellulose I, the native crystalline form typically found in plant-derived fibers. The peak at 22.12° reflects the crystalline structure of the cellulose I polymorph, as indicated by its sharp and narrow profile—features typical of well-ordered crystalline regions [13, 30]. In contrast, the broad hump at 15.83° is associated with amorphous regions, which lack long-range order and thus produce broader peaks [13, 30, 18]. Other cellulose polymorphs, such as cellulose II or III, exhibit different diffraction patterns, but no significant additional peaks corresponding to these forms were observed in this sample, suggesting cellulose I as the dominant polymorph. The crystallinity index of the cellulose microfiber was calculated to be 60.98%, which is typical as this value ranges from 50% to 80% depending on the cellulose source [31]. In a study by Jonjankiat et al. [32], the crystallinity index of the CMF extracted from the sugarcane bagasse treated with nitric acid and sodium hypochlorite was reported to be approximately 50%, which means that the crystallinity index of the CMF produced in this study is relatively higher. However, this is still at the lower end of the typical range for cellulose microfiber as most have crystallinity indexes above 70%. This lower crystallinity could be attributed to the ultrasonication step, as some studies suggest that extensive mechanical fibrillation can decrease crystallinity due to the high shear forces involved that cause scission to the cellulose fibers, leading to a partial collapse of their crystalline structure [33]. Thus, optimizing the mechanical processes to balance high crystallinity and small fiber size is crucial.

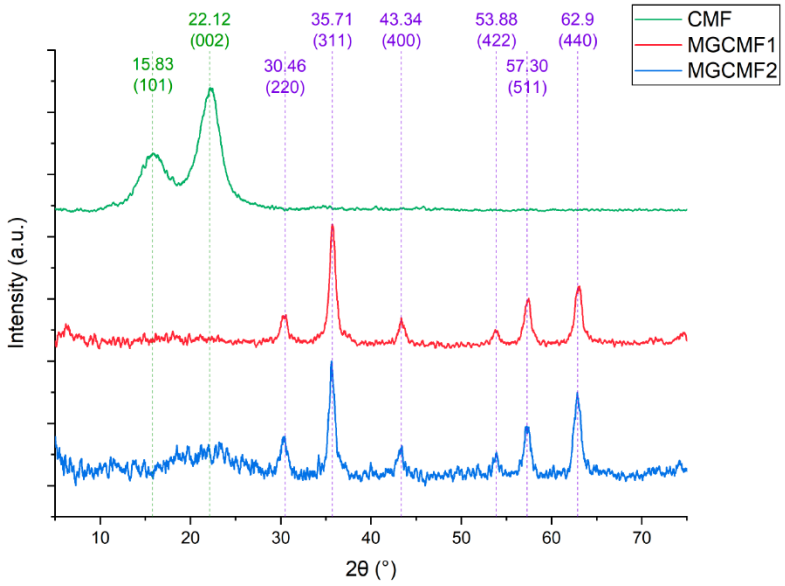

Figure 4. XRD spectra for CMF, MGCMF1, and MGCMF2.

For the MGCMF samples, the six characteristic peaks of the magnetite particles are observed at 2θ values of 30.46°, 35.71°, 43.34°, 53.88°, 57.30°, and 62.90°, corresponding to the (111), (220), (311), (400), (422), and (511) lattice planes of magnetite's inverse cubic spinel structure, respectively [30, 34]. The sharp diffraction peaks also indicate the crystalline nature of the nanoparticles. Using the Scherrer equation, the average particle sizes of the nanoparticles were calculated to be **10.54 ±0.22nm** for the MGCMF1 sample and **10.76 ± 0.18nm** for the MGCMF2 sample, where the uncertainties represent the standard deviation from the sizes calculated across multiple diffraction peaks. These sizes are consistent with literature reports that reported MNP sizes of 11.3nm [35] and 9nm [34].

Additionally, it could be observed that the peaks associated with cellulose are not that visible in the MGCMF samples, although the MGCMF2 sample has a slight peak at 22.12°. This could be due to the high concentration of MNPs in the samples, which may dilute the intensity of the cellulose peaks, particularly since the initial microfiber dispersion was only 0.3% w/v during synthesis. The crystalline structure of the MNPs may also have stronger diffraction peaks that dominate the XRD spectra than the cellulose microfiber [36]. This observation supports the earlier point regarding the need to increase the CMF content during synthesis to ensure it remains detectable after MNP incorporation [36].

3.2. Degradation Efficiency

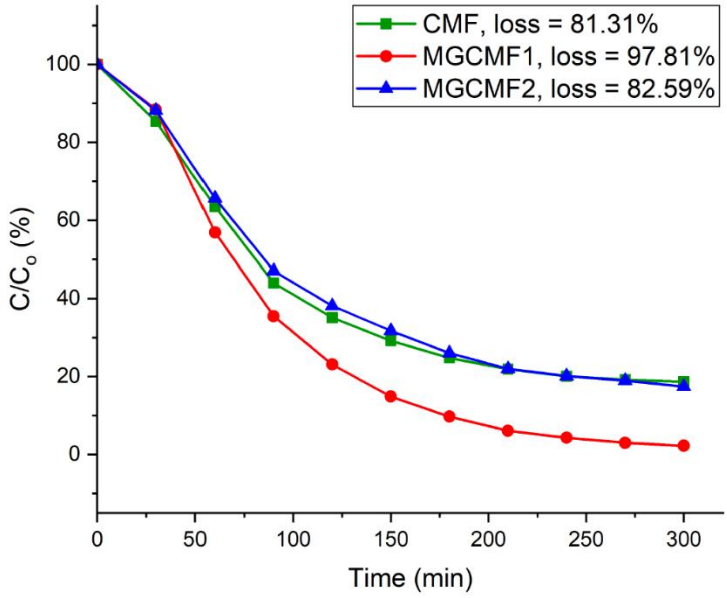

Figure 5. C/Co vs time of CMF, MGCMF1, and MGCMF2.

Figure 5 shows the plot of C/Co with respect to the time, illustrating the degradation efficiency of Rhodamine B in the different catalysts. Among the three specimens tested, MGCMF1 demonstrated the highest efficiency, achieving a 97.81% degradation of RhB in 300 minutes at room temperature. The measured degradation efficiency by MGCMF1 is significant, as it exceeds Amiralian et al. [13] reported 94.9% degradation of Rhodamine B using the magnetite nanoparticle-nanocellulose hybrid at similar time exposures of 300 min at

room temperature. This is encouraging as it confirms that the use of a thicker cellulose fibre does not diminish the composite's efficiency.

Interestingly, the bare CMF and MGCMF2 specimens showed similar degradation profiles to each other, indicating negligible catalytic effects. This deviates from the expected outcome, where a higher concentration of magnetic nanoparticles (MNPs) is expected to result in greater degradation efficiency. MGCMF2, with its higher precursor concentration, should have demonstrated this increased efficiency. However, the poor degradation efficiency of the MGCMF2 sample may be due to the MNP's agglomeration, which formed a compact coating on the surface of the cellulose fiber, leading to fewer active sites and diminished degradation efficiency [37]. MNP's are desired to be well dispersed as this offers maximum surface area for catalytic interaction [13]. The CMF sample also exhibited degradation, however, this may be due to the presence of PMS as it can degrade RhB to a certain degree even in the absence of a catalyst [13].

To statistically validate these observations, a single-factor ANOVA analysis was conducted using **OriginPro** to compare the degradation efficiency of the untreated pure CMF samples and treated MGCMF specimens. Table 1 shows that MGCMF1 exhibited a significantly higher degradation efficiency than the uncatalyzed CMF ($p = 2.64\times10^{-7}$). In contrast, the degradation efficiency of MGCMF2, though slightly higher, was statistically indistinguishable from that of CMF. This means that although both were able to degrade more RhB than the pure CMF sample, only the MGCMF1 sample was able to significantly accelerate the degradation process due to the successful catalytic effect of the MNPs on its surface.

Table 1. Descriptive statistics and ANOVA results reporting the effect of the MNP content on Rhodamine B degradation.

Degradation efficiency	Mean (%, n=12)	Std. Dev. (%)	F crit	P-value	Conclusion (p<0.05)
No MNP content (CMF)	81.3093	0.3120	-	-	-
Low MNP content (MGCMF1)	97.8117	0.2724	7.7086	$2.641\cdot10^{-7}$	significant
High MNP content (MGCMF2)	82.5909	0.6285	7.7086	0.3417	not significant

Figure 6 presents the three kinetics models used to evaluate the catalytic degradation of Rhodamine B (RhB) across the three samples. Based on the models, MGCMF1 sample's degradation is best described by the pseudo-first-order and Langmuir-Hinshelwood models with R^2 values (Table 2) of 0.99584 and 0.98552, respectively. This aligns with the literature, as most studies regarding the catalytic degradation of RhB in sulfate radical-based AOPs typically follow the pseudo-first-order model [38-40]. This means that the concentration of one

of the reactants, which in this case is RhB, plays a significant role in the degradation rate. The Langmuir-Hinshelwood model further supports the idea that the catalytic process involves the adsorption of RhB molecules onto the active sites of the catalyst surface, followed by their degradation. The alignment of the MGCMF1 sample with these models agrees well with the known mechanisms associated with heterogeneous catalysts that demonstrates high degradation efficiency.

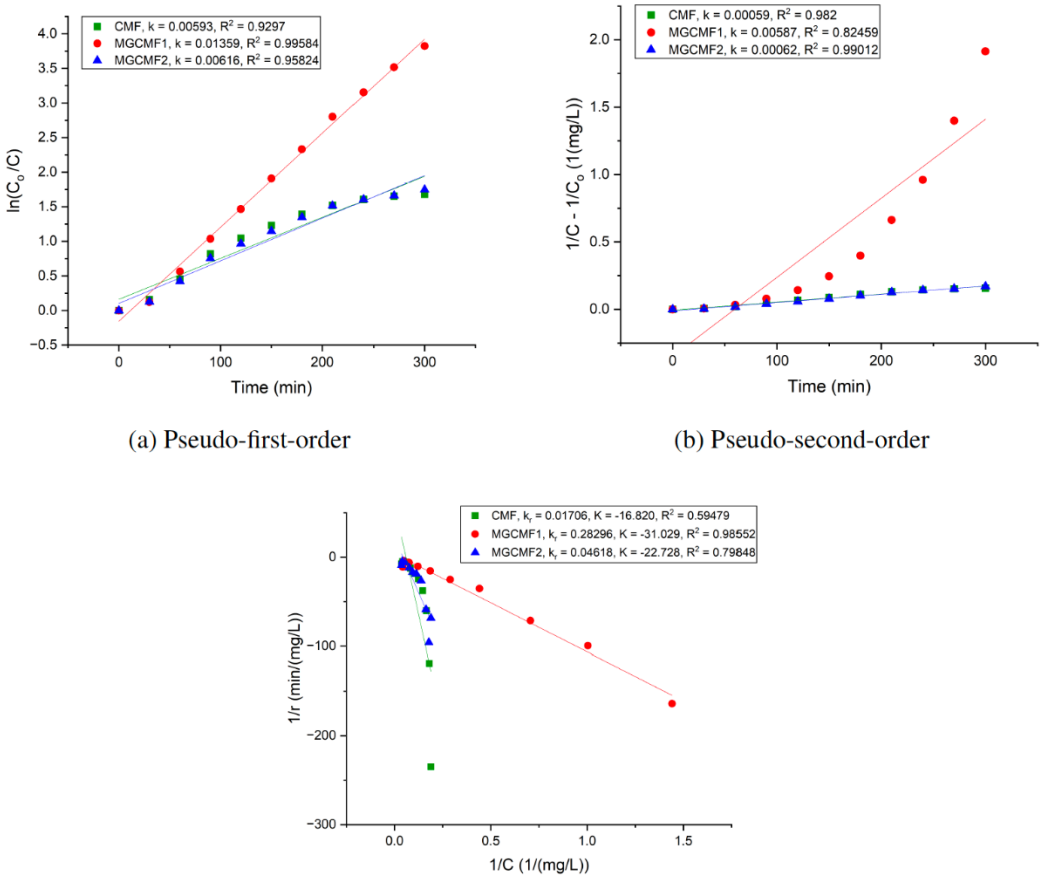

(a) Pseudo-first-order

(b) Pseudo-second-order

(c) Lagmuir-Hinshelwood

Figure 6. Kinetic models for RhB degradation.

On the other hand, the CMF and MGCMF2 samples are best described by the pseudo-second-order kinetic model as their R^2 values (Table 2) are 0.982 and 0.99012, respectively.

Table 2. Kinetic parameters and correlation coefficients (R^2) obtained from the pseudo-first-order, pseudo-second-order, and Langmuir–Hinshelwood models for the degradation of Rhodamine B using CMF, MGCMF1, and MGCMF2.

Kinetic model	Sample	k	R^2
Pseudo-first order	CMF	0.00593	0.92970
	MGCMF1	0.01359	0.99584
	MGCMF2	0.00616	0.95824
Pseudo-second order	CMF	0.00059	0.982
	MGCMF1	0.00587	0.82459
	MGCMF2	0.00062	0.99012
Lagmuir-Hinshelwood	CMF	0.01706	0.59479
	MGCMF1	0.28296	0.98552
	MGCMF2	0.04618	0.79848

Although less common, various literature reports that the kinetics of Fenton oxidation can follow the pseudo-second-order model [38,41]. This assumes that the reaction rate is dependent on the concentrations of two reactants or species. In oxidation reactions, this could mean that the degradation is governed by the interactions between the oxidizing agent (PMS) and the organic compound (RhB) shown in Figure 7.

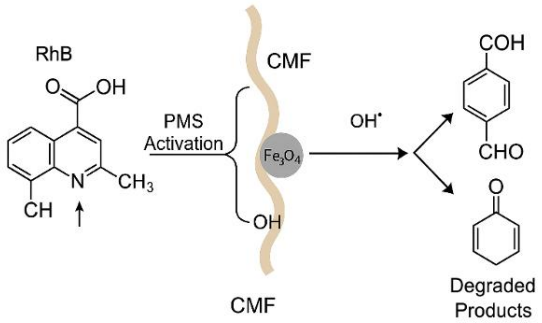

Figure 7. Schematic illustration of the proposed Rhodamine B (RhB) degradation mechanism by magnetite nanoparticle (Fe_3O_4)-functionalized cellulose microfibers (CMFs) via peroxymonosulfate (PMS) activation.

In this study, the distinction between surface-catalyzed and bulk-solution degradation was assessed by comparing reaction rates in the presence and absence of magnetic separation of the catalyst prior to PMS addition, as well as by monitoring changes in degradation efficiency after repeated catalyst use. The negligible loss in activity upon catalyst removal and the similar degradation profiles observed under both conditions indicate that the RhB degradation by these samples is predominantly a bulk solution process rather than a surface-catalyzed one. Additionally, the similar kinetic behavior observed between the CMF and MGCMF2 samples, despite the higher concentration of MNPs in MGCMF2, suggests that the MNPs in MGCMF2 were not effectively utilized. This could be due to potential issues related to surface catalysis, such as MNP agglomeration and deficiency in active sites [37].

IV. CONCLUSION

Magnetite nanoparticles, with particle sizes of approximately 10nm, were successfully synthesized onto the surface of cellulose microfiber derived from sugarcane bagasse. The characterization techniques were able to confirm the presence of both materials. SEM micrographs captured the presence of CMF in the MGCMF membranes, revealing diameter sizes ranging from 4.9 to 18.8μm. The presence of smaller fibrils was also detected with diameters of 0.34 to 0.4μm.

Dye degradation experiments showed MGCMF1 was the most effective catalyst in the OMS-based OAP, registering a RhB degradation efficiency of 97.81% at an exposure time of 300 minutes. In contrast, MGCMF2 were less effective, attributed to MNP agglomeration and the reduction of active catalytic sites. ANOVA analysis further confirmed the superior degradation efficiency of MGCMF1, highlighting the effectiveness of the magnetite nanoparticle synthesis at this concentration. Kinetic analysis revealed that the MGCMF1 degradation process followed the pseudo-first-order and Langmuir-Hinshelwood models, confirming that surface catalysis was the primary mechanism of degradation. Conversely, the CMF and MGCMF2 samples followed pseudo-second-order kinetics, indicating that the degradation process in these samples was more influenced by interactions between the PMS and RhB in the bulk solution.

The findings of this study demonstrate that microsized cellulose fibers can serve as effective templates for MNP, with this combination providing a better degradation efficiency compared to a previously reported MNP-nanocellulose catalyst system. The results also highlight the importance of controlling the amount of MNPs precipitated onto the cellulose surface to prevent the formation of agglomerated MNP structures that may hinder performance. The successful combination of magnetite nanoparticles with cellulose microfiber from local sugarcane bagasse paves the way for developing efficient and sustainable materials for water treatment applications.

V. ACKNOWLEDGEMENT

The authors acknowledge the Office of the Chancellor of the University of the Philippines Diliman, through the Office of the Vice Chancellor for Research and Development, for funding support through the Outright Research Grant (242409 ORG).

References:

[1] Islam MM, Aidid AR, Mohshin JN, Mondal H, Ganguli S, Chakraborty AK. 2025. A critical review on textile dye-containing wastewater: Ecotoxicity health risks, and remediation strategies for environmental safety. Cleaner Chemical Engineering. 11:100165.

[2] O'Shea KE, Dionysiou DD. 2012. Advanced oxidation processes for water treatment. The Journal of Physical Chemistry Letters. 3:2112–2113.

[3] Hodges BC, Cates EL, Kim J-H, 2018. Challenges and prospects of advanced oxidation water treatment processes using catalytic nanomaterials, Nature Nanotechnology. 13:642–650.
[4] Honarmandrad Z, Sun X, Wang Z, Naushad M, Boczkaj G. 2023. Activated persulfate and peroxymonosulfate based advanced oxidation processes (AOPs) for antibiotics degradation – A review. Water Resources and Industry. 29:100194.
[5] Wang J, Wang S. 2017. Activation of persulfate (PS) and peroxymonosulfate (PMS) and application for the degradation of emerging contaminants. Chemical Engineering Journal. 334.
[6] Lim HJ, Kim DJ, Rigby K, Chen W, Xu H, Wu X, Kim JH. 2023. Peroxymonosulfate-based electrochemical advanced oxidation: Complication by oxygen reduction reaction. Environ Sci Technology 57:19054–19063.
[7] Luo H, Zeng Y, He D, Pan X. 2021. Application of iron-based materials in heterogeneous advanced oxidation processes for wastewater treatment: A review. Chemical Engineering Journal. 407:127191.
[8] Fadaei S, Noorisepehr M, Pourzamani H, Salari M, Moradnia M, Darvish Motevalli M, Menglizadeh N. 2021. Heterogeneous activation of peroxymonosulfate with Fe3O4 magnetic nanoparticles for degradation of Reactive Black 5: Batch and column study, Journal of Environmental Chemical Engineering. 9:105414.
[9] Abdelhamid HN. 2024. Nanocellulose-based materials for water pollutant removal: A review. International Journal of Molecular Sciences. 25:8529.
[10] Baruah J, Chaliha C, Kalita E, Nath BK, Field RA, Deb P. 2020. Modelling and optimization of factors influencing adsorptive performance of agrowaste-derived nanocellulose iron oxide nanobiocomposites during remediation of arsenic contaminated groundwater. International Journal of Biological Macromolecules. 164: 53–65.
[11] Olsson RT, Azizi Samir M, Salazar-Alvarez G, Belova L, Ström V, Berglund LA, Ikkala O, Nogues J, Gedde UW. 2010. Making flexible magnetic aerogels and stiff magnetic nanopaper using cellulose nanofibrils as templates. Nature Nanotechnology. 5:584–588.
[12] Carpenter AW, de Lannoy CF, Wiesner MR. 2015. Cellulose nanomaterials in water treatment technologies, Environ Sci Technol. 49:5277–5287.
[13] Amiralian N, Mustapic M, Hossain MSA, Wang C, Konarova M, Tang J, Na J, Khan A, Rowan A. 2020. Magnetic nanocellulose: A potential material for removal of dye from water. Journal of Hazardous Materials. 394:122571.
[14] Ariaeenejad S, Motamedi E, Ramezani Tazehabad M. 2023. Effects of agro–waste resources on characteristics of Fe/nanocllulose hybrids and their applications as novel Fenton-like catalysts in dye removal from wastewater. Process Safety and Environmental Protection. 176:918–933.
[15] Mahmud MA, Anannya FR. 2021. Sugarcane bagasse - A source of cellulosic fiber for diverse applications. Heliyon. 7:e07771.
[16] Saxena S, Moharil MP, Jadhav PV, Ghodake B, Deshmukh R, Ingle AP. 2025. Transforming waste into wealth: Leveraging nanotechnology for recycling agricultural byproducts into value-added products. Plant Nano Biology. 11:100127.
[17] Ahn T, Kim JH, Yang H-M, Lee JW, Kim J-D. 2012. Formation pathways of magnetite nanoparticles by coprecipitation method. The Journal of Physical Chemistry C. 116:6069–6076.
[18] Cullity BD, Stock SR. 2014. Elements of x-ray diffraction. 3rd ed. Essex, England: Pearson Education Limited.
[19] Hozman-Manrique AS, Garcia-Brand AJ, Hernández-Carrión M. Porras A. 2023. Isolation and characterization of cellulose microfibers from Colombian cocoa pod husk via chemical treatment with pressure effects. Polymers. 15:664.
[20] Kumar A, Singh Negi Y, Choudhary V, Kant Bhardwaj N. 2020. Characterization of cellulose nanocrystals produced by acid-hydrolysis from sugarcane Bagasse as agro-aaste. Journal of Materials Physics and Chemistry. 2:1–8.
[21] Hu Z, Zhai R, Li J, Zhang Y, Lin J. 2017. Preparation and characterization of nanofibrillated cellulose from bamboo fiber via ultrasonication assisted by repulsive effect. International Journal of Polymer Science. p. 1–9.
[22] Sacui IA, Nieuwendaal RC, Burnett DJ, Stranick SJ, Jorfi M, Weder C, Foster EJ, Olsson RT, Gilman JW. 2014. Comparison of the properties of cellulose nanocrystals and cellulose nanofibrils isolated from bacteria, tunicate, and wood processed using acid, enzymatic, mechanical, and oxidative methods. ACS Applied Materials & Interfaces. 6:6127-6138.
[23] Shahi N, Min B, Sapkota B, Rangari VK. 2020. Eco-friendly cellulose nanofiber extraction from sugarcane bagasse and film fabrication. Sustainability. 12:6015.

[24] Chandel AK, Antunes FFA, Anjos V, Bell MJV, Rodrigues LN, Singh OV, Rosa CA, Pagnocca FC, da Silva SS. 2013. Ultra-structural mapping of sugarcane bagasse after oxalic acid fiber expansion (OAFEX) and ethanol production by Candida shehatae and Saccharomyces cerevisiae. Biotechnology for Biofuels. 6:4.

[25] Yew YP, Shameli K, Miyake M, Ahmad Khairudin NBB, Mohamad SEB, Hara H, Mad Nordin MFB, Lee KX. 2017. An Eco-friendly mof biosynthesis of superparamagnetic magnetite nanoparticles via marine polymer. IEEE Transactions on Nanotechnology. 16:1047–1052.

[26] Shebanova ON, Lazor P. 2003. Raman spectroscopic study of magnetite (FeFe2O4): A new assignment for the vibrational spectrum. Journal of Solid State Chemistry. 174:424–430.

[27] Slavov L, Abrashev MV, Merodiiska T, Gelev C, Vandenberghe RE, Markova-Deneva I, Nedkov I. 2010. Raman spectroscopy investigation of magnetite nanoparticles in ferrofluids. Journal of Magnetism and Magnetic Materials. 322:1904–1911.

[28] Lee CM, Kubicki JD, Fan B, Zhong L, Jarvis MC, Kim SH. 2015. Hydrogen-bonding network and OH stretch vibration of cellulose: Comparison of computational modeling with polarized IR and SFG spectra. The Journal of Physical Chemistry B. 119:15138–15149.

[29] Senapitakkul V, Vanitjinda G, Torgbo S, Pinmanee P, Nimchua T, Rungthaworn P, Sukatta U, Sukyai P. 2020. Pretreatment of cellulose from sugarcane bagasse with xylanase for improving dyeability with natural dyes. ACS Omega. 5:28168–28177.

[30] Dang B, Chen Y, Wang H, Chen B, Jin C, Sun Q. 2018. Preparation of high mechanical performance nano-Fe_3O_4/wood fiber binderless composite boards for electromagnetic absorption via a facile and green method. Nanomaterials (Basel). 8:52.

[31] Khenblouche A, Bechki D, Gouamid M, Charradi K, Segni L, Hadjadj M, Boughali S. 2019. Extraction and characterization of cellulose microfibers from Retama raetam stems. Polímeros. 29.

[32] Jonjankiat S, Wittaya T, Sridach W. 2011. Improvement of poly (vinyl alcohol) adhesives with cellulose microfibre from sugarcane bagasse. Iranian Polymer Journal. 20:305–317.

[33] Ni Y, Li J, Fan L. 2021. Effects of ultrasonic conditions on the interfacial property and emulsifying property of cellulose nanoparticles from ginkgo seed shells. Ultrason Sonochem, 70:105335–105335.

[34] Fan H-L, Zhou S-F. Jiao W-Z, Qi G-S, Liu YZ. 2017. Removal of heavy metal ions by magnetic chitosan nanoparticles prepared continuously via high-gravity reactive precipitation method. Carbohydrate Polymers. 174:1192–1200.

[35] Viltres H, Odio OF, Borja R, Aguilera Y, Reguera E. 2017. Magentite nanoparticle for arsenic remotion. Journal of Physics. Conference Series. 792:012078.

[36] de Castro Alves L, Cerqueira MA, González-Goméz MA, Garcia-Acevedo P, Prieto ÁA, Piñeiro Redondo Y, Pastrana L, Rivas J. 2024. Innovative films by embedding magnetic nanoparticles in cellulose acetate. Food Packaging and Shelf Life. 42:101264.

[37] Mzimela N, Tichapondwa S, Chirwa E. 2022. Visible-light-activated photocatalytic degradation of rhodamine B using WO(3) nanoparticles. RSC Adv. 12:34652–34659.

[38] Aljuboury DAdA, Palaniandy P. 2017. Kinetic study of inorganic carbon (IC) removal and COD removal from refinery wastewater by solar photo-Fenton. Global NEST Journal. 19:641–649.

[39] Hu L, Deng G, Lu W, Lu Y, Zhang Y 2017. Peroxymonosulfate activation by Mn 3 O 4 /metal-organic framework for degradation of refractory aqueous organic pollutant rhodamine B. Chinese Journal of Catalysis. 38:1360–1372.

[40] Xia X, Zhu F, Li J, Yang H, Wei L, Li Q, Jiang J, Zhang G, Zhao Q. 2020. A Review study on sulfate-radical-based advanced oxidation processes for domestic/industrial wastewater treatment: Degradation, efficiency, and mechanism. Front Chem. 8:592056–592056.

[41] El Haddad M, Abdelmajid R, Rachid L, Rachid M, Nabil S. 2014. Use of Fenton reagent as advanced oxidative process for removing textile dyes from aqueous solutions. Journal of Materials and Environmental Science. 5:2028–2508.